Journal of *Marine Science and Engineering*

MDPI

Article

Experimental Study on Motion Characteristics of Cavity Attached to the Tail of Underwater Vehicle

Xiongliang Yao [1,2], Zhaoyu Qu [1,2,*], Guihui Ma [1,2,*], Nana Yang [1,2], Xiaobo Quan [2,3] and Shaohua Cheng [1,2,3]

[1] College of Shipbuilding Engineering, Harbin Engineering University, Harbin 150001, China; xiongliangyao@hrbeu.edu.cn (X.Y.); yangnana@hrbeu.edu.cn (N.Y.); chengshaohua_2008@163.com (S.C.)
[2] Innovation Center for Cross-Media Aircraft Technology, Harbin 150001, China; xiaoboq1976@126.com
[3] China Academy of Launch Vehicle Technology, Beijing 100076, China
* Correspondence: quzhaoyu@hrbeu.edu.cn (Z.Q.); maguihui@hrbeu.edu.cn (G.M.)

Abstract: The formation and development of an attached cavity at the tail of an underwater moving vehicle involves a complex multiphase flow, which determines the load characteristics and motion stability of the vehicle. In this study, an experimental method was used to explore the formation process and motion characteristics of the cavity at the tail of the vehicle, and a pressure sensor installed at the tail of the model was used to establish the relationship between the evolution of the tail attachment cavity and transient pressure. The study found that the process of pulling and breaking the attached cavity was accompanied by the generation of bidirectional jets, and reducing the cavitation number could weaken the occurrence of jet impact. When the ventilation flow reaches the critical value $\overline{Q}_{in}$ = 1.28, the cavity pulsates. In addition, increasing the ventilation flow does not increase the size of the tail cavity, and the length of the cavity at the closure increases with the decrease of the cavitation number.

Keywords: underwater vehicle; tail attachment cavity; pressure characteristics; entrainment mechanism

check for updates

Citation: Yao, X.; Qu, Z.; Ma, G.; Yang, N.; Quan, X.; Cheng, S. Experimental Study on Motion Characteristics of Cavity Attached to the Tail of Underwater Vehicle. *J. Mar. Sci. Eng.* **2023**, *11*, 1287. https://doi.org/10.3390/jmse11071287

Academic Editor: Alon Gany

Received: 16 May 2023
Revised: 9 June 2023
Accepted: 16 June 2023
Published: 25 June 2023

Copyright: © 2023 by the authors. Licensee MDPI, Basel, Switzerland. This article is an open access article distributed under the terms and conditions of the Creative Commons Attribution (CC BY) license (https://creativecommons.org/licenses/by/4.0/).

1. Introduction

An underwater vehicle usually uses high-pressure gas ejection to achieve water movement. After the vehicle is out of the launcher, the high-pressure gas used as a power source will form an independent attached tail cavity at the tail of the vehicle, and the tail cavity will undergo pulsation. Processes such as shedding and collapse substantially affect the hydrodynamic load and motion stability of a vehicle, so they have been extensively studied in the field of fluid dynamics [1–6]. However, the vertical motion of an attached cavity acts as a complex unsteady flow with multiphase participation and fluid–structure interaction [7–10].

In the past, a series of basic scientific research work has been conducted on the motion characteristics of cavities in liquids [11–14], determining the dynamic behavior of bubbles in different viscous liquids. It was found that for the bubbles under the action of walls, the perturbation range of the bubbles is substantially concentrated, increasing the velocity gradient around the bubble. On this basis [15], through further experimental studies, the bubble formation mechanism under the interaction between the bubble and wall was studied, and a theoretical model was established to predict the bubble formation process, consistent with the experimental results.

For underwater vehicles, the attachment of a cavity can usually be divided into two types. One type of attachment is that the cavity is attached to the surface of the vehicle to form a fully wrapped supercavity [16], and the other type of attachment is that the cavity is attached to the tail of the vehicle to form an independent attachment cavity. For the first type of cavity attachment, the effect of wall is undoubtedly important. A vehicle in the all-wet state has a large traveling resistance due to the viscous action of the liquid [17,18]. The use of gas ventilation can make the entire surface of the vehicle covered with a layer

of gas film, achieving a good drag reduction effect [19–21]. Through further water tunnel tests [22,23], it was found that an increase in ventilation volume can improve the stability of the cavity and reduce the load on the test body. This shows that the attached cavity on the surface of the vehicle substantially affects the motion of the vehicle. Aiming at the second type of cavity attachment, Xu et al. [24] obtained a horizontal tail attachment cavity of a vehicle using a nozzle jet in a water tunnel experiment. The instantaneous and time average shapes of ventilated cavity under different Froude number and ventilation flow rate were summarized. This study focuses on the second type of cavity attachment in the state of vertical unconstrained motion.

In a ventilated cavity flow, entrainment and vortex are the problems that need to be solved [25–28]. Moudjed et al. [29] changed the vortex structure by adding obstacles and found that the use of large obstacles can easily lead to gas entrainment with a lower suction velocity. Spurk et al. [30] further deduced the effect of gas temperature on gas loss in a ventilation cavity and extended the theory of gas loss in the ventilation cavity under isothermal conditions to nonisothermal conditions, consistent with the experimental results. Yu et al. [31] revealed the correlation mechanism between ventilation and vortex evolution through a large eddy simulation. The results show that the formation of a U-shaped cavity is closely related to the separation of re-entrant jet and the effect of vortex evolution. As a common phenomenon in ventilated cavity flow, re-entrant jet is also the focus of many studies. Kinzel et al. [32] found that a re-entrant jet caused wake instability and cavity pulsation. Jiang et al. [33] further investigated the evolution model of a ventilated cavity using experimental methods and found that the transfer of the residence position of gas jet from a potential core area to the turbulent zone of the jet is the reason for cavity transformation.

However, at this stage, studies have mainly explored the flow characteristics of an attached cavity by conducting water tunnel tests, and there are few studies on the interaction between a free-moving body and cavities. In particular, less attention has been paid to specific problems such as gas breaking and backfire flow during the formation of an attached cavity at the tail of the vehicle. Therefore, it is of practical significance to further elucidate the formation mechanism and motion characteristics of tail attachment cavity through experiments. Because it is closer to reality and has a better engineering background, it can provide guidance for the study of cavitation flow. In this study, through an experimental comparison, the effects of different cavitation numbers and ventilation volumes on the formation mechanism of tail attachment cavity were analyzed, and the flow characteristics of the cavity were further analyzed.

2. Experimental Setup

In this experiment, based on a small-scale vacuum water tank test device of Harbin Engineering University, the motion characteristics of a cavity attached to the tail of a vehicle were studied by high-pressure gas ejection. The device includes a decompression system, a control system, an information collection system, and other auxiliary equipment, as shown in Figure 1.

The decompression system is composed of a test tank and vacuum pump (YE3-100L-2T, Shandong Zhonggong Motor Co., Ltd., Zibo, China). The maximum pumping capacity of the vacuum pump can reach an absolute pressure of 10 kPa. The test tank is in the shape of a column, with observation windows located on its central shooting surface and back and right wall; the top is connected to a vacuum pump through a valve. In the test, the water in the test tank is left standing for a long enough time to keep the temperature consistent with the indoor environment, and free bubbles in the water can be eliminated at the same time. The test model was installed in a launcher, and the air tightness was ensured by using a rubber sealing ring. The gap between the inner wall of launcher and the shell of vehicle is very small and can be ignored. The launch cylinder was fixed in the center position at the bottom of test tank through a support.

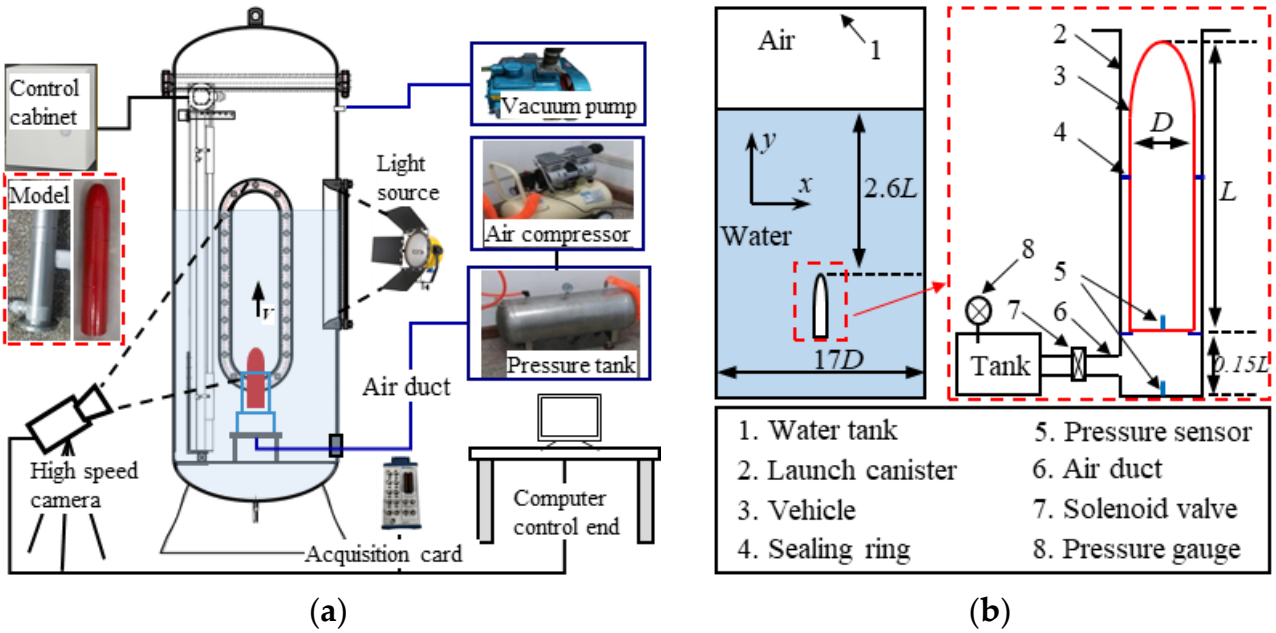


Figure 1. Schematic diagram of experimental equipment (**a**) and magnification diagram of vehicle (**b**).

The control system includes a control cabinet, gas tank, and pressure gauge (ISE30A-01-P-L, SMC). The gas tank is connected with the launcher inside the water tank through a solenoid valve. Solenoid valve response time is about 20 ms. The maximum pressure of the gas tank is 1.2 MPa. Controlling the opening and closing time of the solenoid valve adjusts the $\overline{Q}_{in}$. The length of the vehicle body is L = 320 mm. The vehicle slenderness ratio remains unchanged, which is $L/D = 5.65$, D is the diameter of the vehicle. The distance between the mouth of the launching cylinder and the water surface is about 2.6L. In the test, gas with a certain pressure is added to the gas tank, and the opening and closing time of solenoid valve was controlled using a control cabinet by passing a certain amount of high-pressure gas into the launcher in a short time to provide a traveling power for the vehicle.

In general, the gas intake problem in this study can be regarded as an isothermal process [34]. Therefore, the ideal gas equation of state can be used to describe the gas state in the gas tank before and after the test, and the gas quality can be obtained.

The information acquisition system is mainly composed of a computer, data acquisition instrument, pressure sensor, and Phantom VEO-640S high-speed camera. The camera observes the movement of the model at a sampling frequency of 4000 fps. A pressure sensor (CYG1505ALLF, Kunshan Shuangqiao Sensor Measurement and Control Technology Co., Ltd., Suzhou, China) was installed in the center position of the bottom of the launcher and the center position of the bottom of the vehicle, and the sampling rate was set to 20 kHz.

Before the test, water was injected into the test tank and filled to the top of the observation window to ensure that the test model had enough movement stroke. During the experiment, the control system controls the solenoid valve to open and close to provide the driving power for the vehicle, and a high-speed camera captures the movement of the vehicle through the observation window in the test tank and records the development of the cavity. The pressure sensor provides the pressure data in the launcher and at the bottom of the body using a data acquisition system.

3. Results and Discussion

3.1. Formation and Evolution Characteristics of Tail Attachment Cavity

An underwater vehicle obtains the underwater kinetic energy through the ejection of a high-pressure gas in the launcher, and a part of the gas in the launcher will form an attachment cavity at the tail of the vehicle.

In this paper, the motion characteristics of the tail attachment cavity of the vehicle are studied by means of experimental methods. In the process of underwater high-pressure gas ejection vehicle motion, the isothermal process is usually applied without considering the influence of energy and temperature. In order to better understand the relationship between the control parameters and the test results, the control parameters of the attached cavity length are derived as follows:

$$L_B = f(t, \rho_w, v, \mu, h, P_\infty, P_v, g, L, m, \rho_a, S, f, V, V_b) \tag{1}$$

where L_B is the length of the tail attachment cavity, t is the motion time, ρ_w is the water density, v is the motion velocity of the vehicle, μ is the kinematic viscosity coefficient of water, h is the water depth, P_∞ is the ambient pressure, P_v is the saturated vapor pressure of water, g is the gravitational acceleration, L is the length of the vehicle, m is the mass of the gas through, ρ_a is the density of the gas through, S is the surface tension coefficient, f is the bubbles shedding frequency, V is the vehicle volume, V_b is the bubble volume.

Selecting time t, water density ρ_w, vehicle length L as the basic parameters, the equation above can be transformed into the following dimensionless form:

$$\frac{L_B}{L} = f\left(\frac{tv}{L}, \frac{\rho_w v L}{\mu}, \frac{h}{L}, \frac{P_\infty - P_v}{0.5\rho_w v^2}, \frac{v}{\sqrt{gL}}, \frac{m}{\rho_w L^3}, \frac{\rho_a}{\rho_w}, \frac{\rho_w v^2 L}{S}\right) \tag{2}$$

where $\frac{tv}{L}$ is the dimensionless time ($\overline{T}$), which can be further converted to $\frac{fL}{v}$, i.e., the Strouhal number, $\frac{\rho_w v L}{\mu}$ is the Reynolds number, $\frac{h}{L}$ is the dimensionless water depth, $\frac{P_\infty - P_v}{0.5\rho_w v^2}$ is the cavitation number (σ), $\frac{v}{\sqrt{gL}}$ is the Froude number (Fr), $\frac{\rho_w v^2 L}{S}$ is the Weber number. $\left(\frac{m}{\rho_w L^3} / \frac{\rho_a}{\rho_w}\right) / \frac{tv}{L} = \frac{m}{\rho_a t v L^2}$ is the dimensionless incoming air volume $\overline{Q}_{in}$. In addition, we define other dimensionless parameters. $\overline{H} = h/L$ is the dimensionless displacement of the model movement, $\overline{V}_b = V_b/V$ is the dimensionless volume of the bubble, $\overline{Y}$ is the dimensionless displacement of the model movement, $\overline{Y} = y/L$, among them, y is the displacement of the vehicle, $\overline{U}$ is the dimensionless velocity of the model movement, $\overline{U} = v/U_{max}$, U_{max} is the maximum moving speed of the vehicle.

In fact, when the motion characteristics of the tail attachment cavity are explored by means of a high-pressure gas ejection vehicle, we usually think that the inertial force is dominant, so the influence of the Weber number and the Reynolds number is ignored. In addition, changing the size of the ventilation flow rate $\overline{Q}_{in}$ dramatically changes the vehicle Froude number. Therefore, this paper focuses on exploring the influence of the ventilation flow rate on the motion characteristics of the tail attachment cavity.

In order to better explore the formation and motion characteristics of the tail attachment cavity of the vehicle, the research cases in this paper are shown in Table 1. Among them, the Froude number and the cavitation number are the values at the time when the vehicle leaves the launch tube. This section explores case 1 first, in which ventilation for $\overline{Q}_{in} = 1.54$. Regarding the tail attachment cavity movement characteristics, the typical moment of cavity pulsation is shown in Figure 2. The initial Froude number and cavitation number at the time when the vehicle leaves the launcher are obtained, which are $Fr = 17.4$, $\sigma = 1.11$, respectively. From the evolution process of the tail attachment cavity, it can be found that the formation and movement of the attachment cavity can be divided into two stages.

Table 1. Experiment case.

Number	$\overline{Q}_{in}$	$p_0/\rho g h_0$	*Fr*	σ
1	1.54	12.26	17.4	1.11
2	1.34	12.26	16.07	1.26
3	1.28	12.26	15.94	1.29
4	1.15	12.26	15.4	1.41
5	1.02	12.26	12.91	2.01
6	1.02	7.14	17.22	0.64
7	1.02	4.96	21.15	0.43
8	0.77	1.57	8.34	0.86
9	1.28	2.54	16.9	0.21

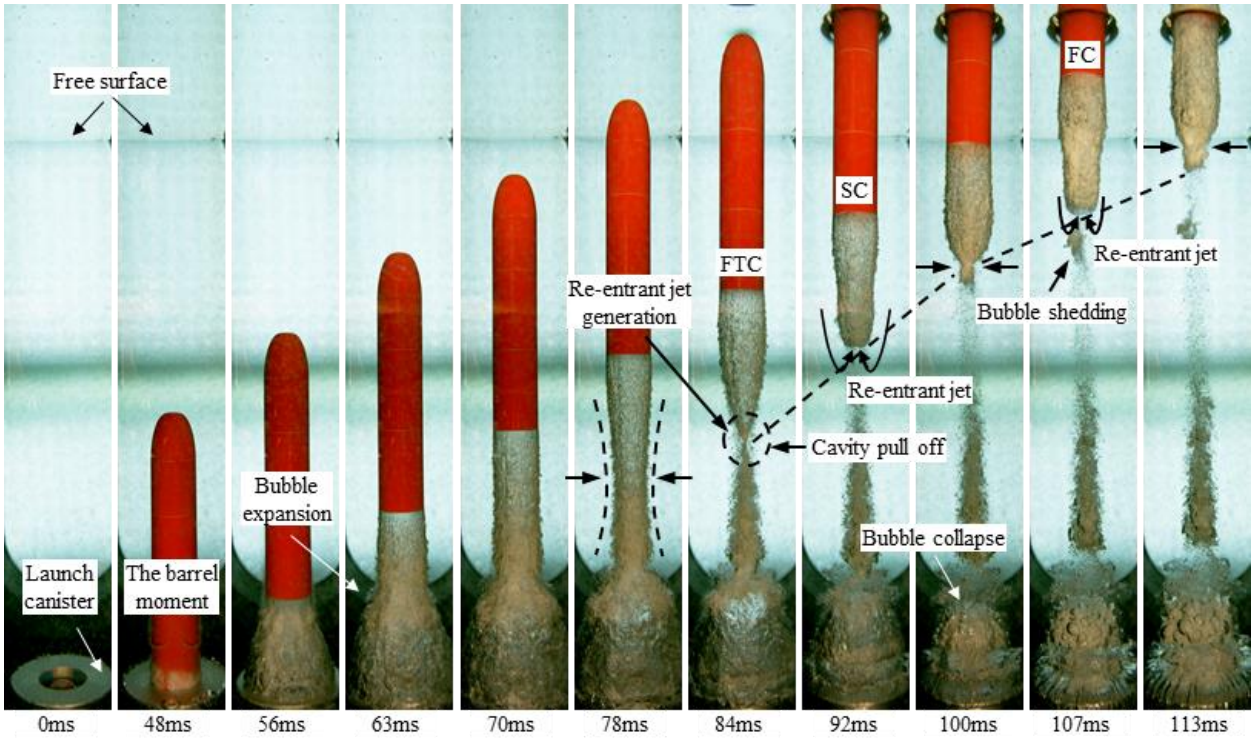


Figure 2. Evolution characteristics of tail attachment cavity in case 1, where $\overline{Q}_{in} = 1.54$, $Fr = 17.4$, and $\sigma = 1.11$.

Tail attachment cavity formation (0–84 ms): A launcher is filled with a certain flow of high-pressure gas in a short time, and the vehicle achieves the kinetic energy under the action of high-pressure gas and quickly leaves the launcher. Because of a high gas pressure in the launcher, the local water depth pressure is less than the gas pressure in the launcher. When the vehicle moves to the position of the launcher mouth, the cavity at the launcher outlet expands rapidly, and the cavity size exceeds the diameter of the launcher. At this time, the vehicle is located above the cavity, and the velocity does not decay, indicating that the expansion of cavity still provides kinetic energy for the vehicle. At the same time, a part of the gas is attached to the tail of the vehicle by forming a tail attachment cavity. At this time, the attached cavity at the tail of the vehicle has a cylindrical shape, and the attached cavity is limited by the diameter of the vehicle. The diameter of the cavity is the same as that of the vehicle. During rising, the cavity size is further lengthened; thus, the cavity cannot maintain the shape of the cylinder, resulting in a necking phenomenon. With the continuation of vertical motion of the vehicle, the necking phenomenon is intensified, and the cavity is broken. We define the cavity shape as a fully transparent cavity (FTC).

Cavity pulsation process (84–113 ms): Because of a continuous vertical motion of the vehicle, the columnar cavity cannot maintain a cylindrical shape, leading to the cavity

breaking phenomenon. At the moment of cavity breaking, the end closure of the attached cavity shows a white foam shape accompanied by the re-entrant jet phenomenon and rapidly develops to both the ends of the cavity fracture. The cavity formed at the outlet of the launcher and the re-entrant jet rushes toward the tail of the vehicle, causing a periodic pulsation of the cavity. The pulsation period is shown in Figure 3. In the pulsating process, the end of the bubble is narrowed under the action of the re-entrant jet, and the cavity formed is a shrinking cavity (SC). At the same time, the action of the jet makes a large amount of water enter the cavity, and under the joint action of cavity breaking and contraction, a part of the gas at the bottom of the cavity is squeezed to the upper end of the cavity. Thus, the radial size of the upper end of the cavity expands, and the lower end contracts. Because of a remarkable scouring effect of the incoming flow, the radially expanding cavity cannot maintain the expansion state and moves downwards and contracts. When the re-entrant jet hits the tail of the vehicle, it is blocked from spreading to the circumferential direction. This further increases the gas and water content in the cavity and changes the gas distribution inside the cavity, thus forming unstable fluctuations on the surface of the cavity.

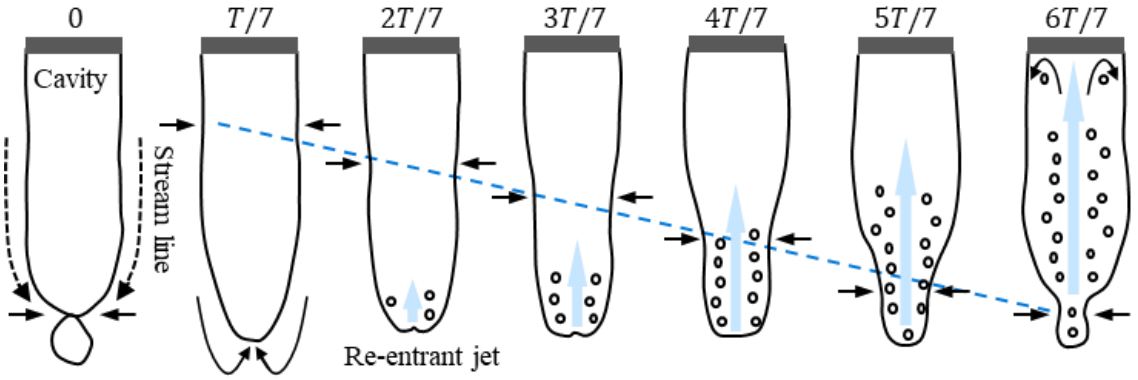


Figure 3. Schematic diagram of cavity pulsation cycle.

Because the gas at the end of the cavity is not completely entrained into the cavity during the entrainment, a gas pinch off is caused by the shedding phenomenon. At the same time, we can observe that the end of the cavity exhibits a twin-vortex pattern. The secondary pulsation followed, accompanied by the secondary jet impact; the entrainment phenomenon at the end of the cavity was obvious. After the entrainment was completed, the cavity pinch off and fall off phenomenon occurs again. We defined the cavity shape at this time as foam cavity (FC).

During the entire movement process, the cavity has two times of pulsation, two times of jet impact, and two times of gas pinch off and fall off. The initial pulsation is accompanied by the generation of a jet. The pulsation period is T = 13.5 ms and 11.9 ms in turn. Obviously, the pulsation period decreases with the decrease in water depth. The tail attachment cavity is always attached to the tail of the vehicle, and there is no state where the cavity floats over the tail of the vehicle.

Therefore, when the pressure inside the cavity is less than the ambient pressure, the balance between the inertial force and the pressure causes the cavity to bend inward. As a result, the curvature radius of the cavity is reduced, which promotes the liquid to shoot into the cavity and form the re-entrant jet.

For the flow characteristics of the tail attachment cavity of an underwater vehicle, its cavity length is one of its important parameters. The length of the cavity refers to the length from the point of separation to the point where the cavity closes. During the measurement, it is affected by a large number of uncertain factors due to the instability of the closed region. By measuring the length of the attached cavity at the tail of the vehicle after the cavity is broken, the measurement error was obtained, as shown in Figures 4 and 5.

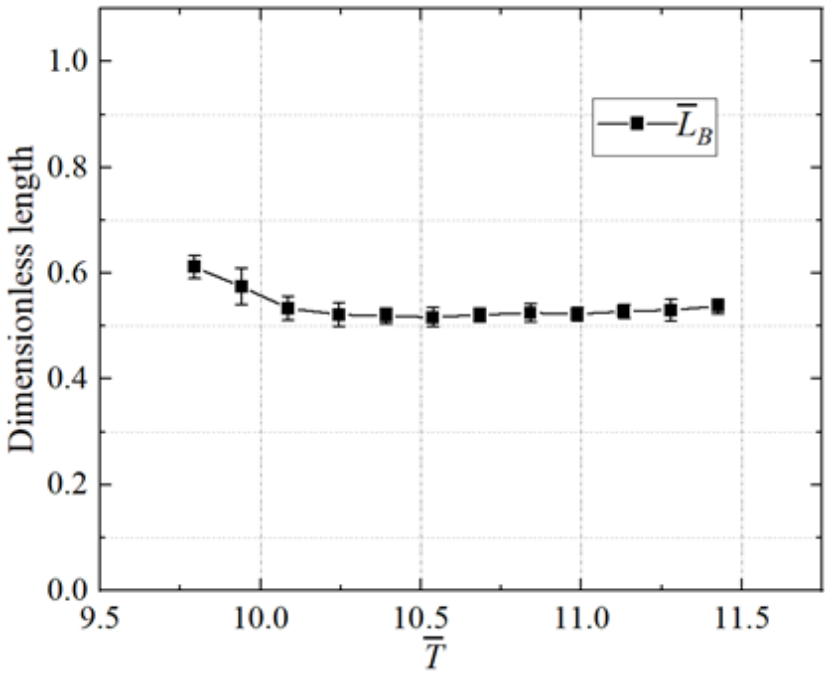


Figure 4. Variation curve of tail-attached cavity length.

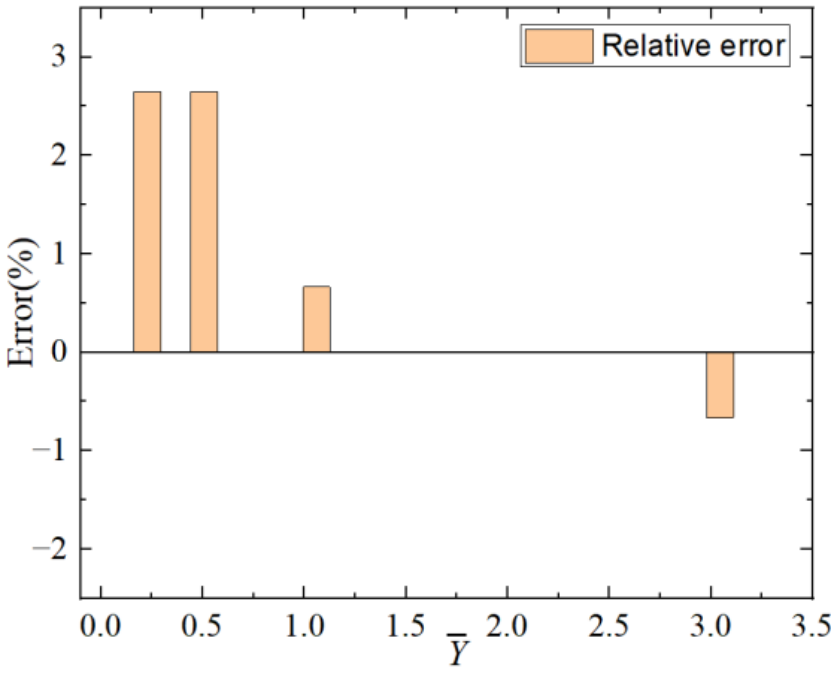


Figure 5. Relative error of diameter measurement of underwater vehicle.

Figure 4 shows that the size of the cavity decreases after breaking, and the size changes slightly during the ascent of the vehicle. At the same time, it was found that the error fluctuation of the cavity size data measured by the test is small, indicating that the test of motion characteristics of the cavity attached to the tail of the vehicle is reliable. The relative error caused by measuring different displacement position data during the movement of the vehicle was further analyzed. In fact, this is due to the error caused by the shooting angles of the vehicle at different displacements during the shooting. Therefore, it is of great significance to evaluate the relative error caused by the displacement change. Figure 5 shows that the maximum relative error of the model diameter measurement under different

displacements does not exceed 3%, indicating that the measurement of the cavity length in the experiment is accurate and acceptable. In fact, to photograph the complete process of the motion of the vehicle, the shortest distance between the camera and the model is larger than the displacement of the model, so we can ignore the measurement error caused by the shooting angle.

The change in speed during the movement of the vehicle was analyzed, as shown in Figure 6. In the early stage of the motion of the vehicle, the speed increases rapidly, and then the rate of speed increase slows down, but before the vehicle leaves the launcher outlet, the speed is always accelerated. When the vehicle is separated from the launch cylinder, the gas in the cylinder expands rapidly, and the speed of the vehicle remains accelerated at this time, indicating that the gas expansion process has a driving effect on the vehicle. When the air mass at the outlet of the launcher expands to the maximum, the speed of the vehicle reaches the maximum. Subsequently, the cavity at the tail of the vehicle was separated from the air mass at the mouth of the tube and lost the continuous propulsion of the launched air mass to the vehicle. At the same time, the vehicle was affected by the resistance of the water body during the movement, and its speed decreased.

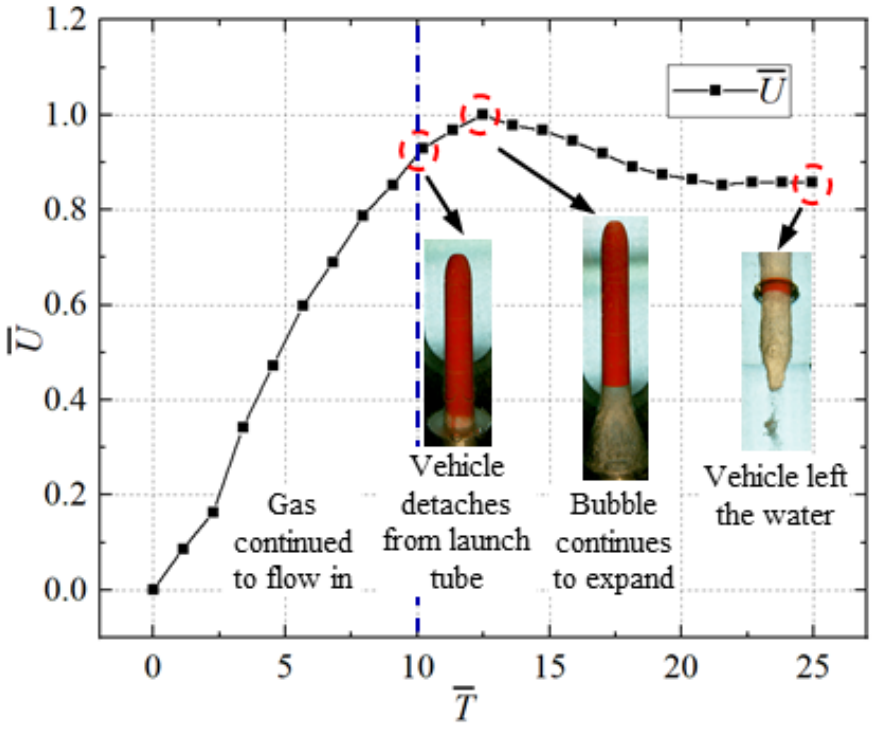


Figure 6. Variation curve of vehicle speed.

3.2. Analysis of Pulsation of Tail Attachment Cavity at the Tail of Vehicle

The pressure change of the cavity during movement has always been the focus of many studies. To better illustrate the motion characteristics of the tail attachment cavity, this section continues to analyze the pressure variation of the tail attachment cavity of the vehicle under case 1 by installing pressure sensors at the center of the bottom of the vehicle. The pressure data of the tail attachment cavity recorded by the pressure sensor at the tail of the vehicle were compared with the pressure data at the center point at the bottom of the launching cylinder, as shown in Figure 7.

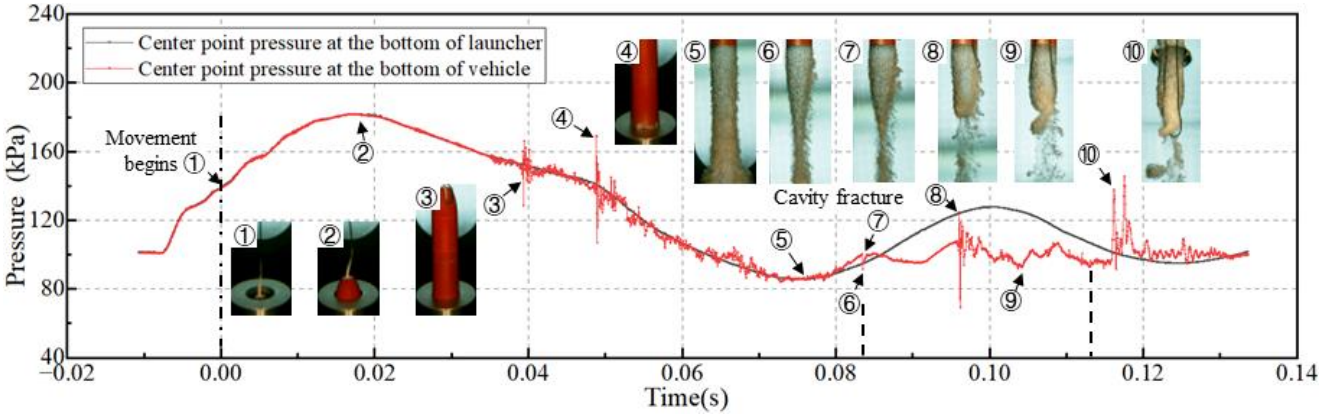


Figure 7. Cavity pressure analysis in case 1.

Figure 7 shows that with the increase in ventilation pressure inside the launcher, at time ①, it is the initial moment of displacement of the vehicle, and the pressure at the tail of the vehicle is consistent with that in the launcher. When the displacement of the vehicle reaches $\overline{Y} = 0.15$ (②), the pressure peak reaches the maximum. When the vehicle moves to the position of the sealing ring (③), a part of the water body enters the launcher, and the pressure changes suddenly, accompanied by pressure shock. When the vehicle moves to the position of the outlet of the launcher (Figure 7, ④), a small amount of gas has rushed out of the launcher under the action of high pressure, and a gas film is formed at the bottom of the vehicle, accompanied by a strong pressure shock, which is mainly caused by the expansion of high-pressure gas. As the vertical displacement of the vehicle continues, the gas in the launcher adheres to the tail of the vehicle, and the cavity at the tail is columnar. Under the stretching action of the vertical motion of the vehicle, the air mass at the outlet of the launcher is further expanded, and the internal pressure of the cavity continues to decrease. Notably, when the vehicle is separated from the launcher, the pressure reduction rate in the cavity increases substantially. This is because the cavity is not hindered in the radial direction, and the volume expansion of the cavity is further developed.

At the same time, under the action of inertia, the volume of air mass at the outlet of the launcher expands to the maximum, and the pressure reaches the lowest point (⑤) at this time. The internal pressure of the cavity is substantially lower than the local water depth pressure. At this time, under the squeezing action of the surrounding water body, the radial dimension of the cavity shrinks, and the internal pressure of the cavity increases. With the continuous vertical motion of the vehicle, the radial shrinkage of the cavity is further intensified. At the same time, due to insufficient ventilation, the columnar cavity cannot maintain its own shape, and the "necking" phenomenon occurs.

With the intensification of the necking phenomenon, the attached cavity at the tail further shrinks due to the traction effect of the vehicle and the extrusion of the surrounding water body, while the air mass of the launcher outlet is larger in size and has no traction effect on the vehicle. Therefore, the pressure rise rate is lower than that of the attached cavity at the tail. When the shrinkage reaches a certain level, the columnar cavities cannot maintain their own shape and rupture, accompanied by a sudden drop in the pressure inside the cavity (⑥). At this time, the local water depth pressure is substantially greater than the internal pressure of the cavity. Then, jets are rapidly generated under the action of pressure difference at the closed position of the cavity (⑦), and the jets impact the tail of the vehicle and the bottom of the launcher, respectively, in the axial direction. The so-called re-entrant jet phenomenon is formed for the attached cavity at the tail of the vehicle. The impact of re-entrant jet on the tail of the vehicle causes a sudden increase in pressure, which is accompanied by unstable fluctuations in pressure.

With a periodic pulsation of the tail attachment cavity, the internal pressure of the cavity also shows regular fluctuations, because of the periodic pressure fluctuations gener-

ated by the periodic changes in the volume during the pulsation of the cavity. The cavity is accompanied by the occurrence of air mass shedding during the pulsation (⑨), and the shedding time is at the minimum of pressure fluctuation. At this point, the end of the cavity is closed, and a secondary jet is generated immediately.

When the vehicle moves to the water surface (⑩), continuous pressure shocks occur. This shows that when the cavity is separated from the water medium, because of a sudden drop in pressure, the local water depth pressure at the underwater cavity is greater than the internal pressure of the cavity, and the intensity of generated re-entrant jet increases, causing a continuous impact load on the tail of the vehicle. The peak value of shock pressure is about 1.2–1.4 times of the local water depth pressure, and the pulse width is about 0.4 ms.

In order to better analyze the characteristics of cavity pulsation frequency, this paper conducts Fourier transform on the pressure data after the cavity is pulled off to obtain the spectrum of pressure pulsation, as shown in Figure 8. From the frequency domain analysis, it can be clearly found that the low frequency peak is about 40 Hz, while the high frequency peak is about 130 Hz.

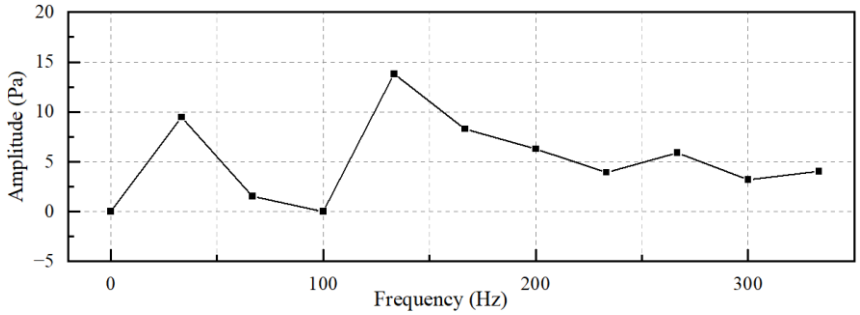


Figure 8. Spectral analysis of pressure pulsation of cavity after the ⑥ time.

Obviously, the jet impact generated during cavity breaking has an important influence on cavity pressure pulsation. To better observe the effect of jet impingement on cavity dynamics, we evaluated the relationship between different ventilation flow rates and cavity morphologies, and selected cases 1–4 for comparison, as shown in Figure 9. It can be observed that with the decrease in ventilation flow, the size of the cavity at the outlet of the launcher decreases substantially, and the position where the cavity breaks down also decreases. The jet occurs at the initial moment when the cavity breaks.

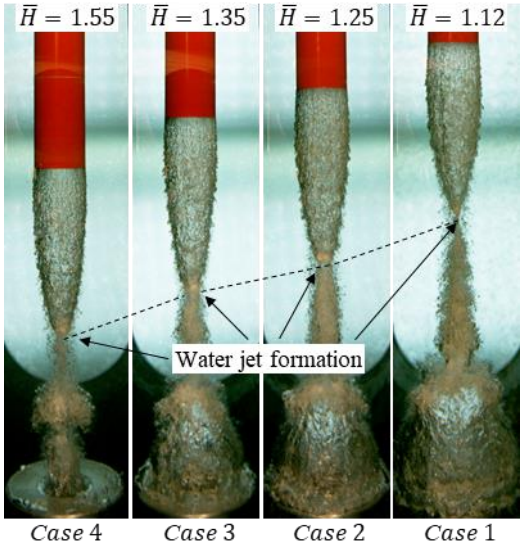


Figure 9. Comparison of cavity breaking positions under different ventilation volume amounts.

When the vehicle moves with the same displacement, the impact shape of re-entrant jet on the cavity changes substantially, as shown in Figure 10. The re-entrant jet impingement distance increased substantially with decreasing ventilation flow. When the ventilation flow reaches the critical value $\overline{Q}_{in} = 1.28$, the cavity pulsation phenomenon occurs. This indicates that when the flow rate is greater than $\overline{Q}_{in} = 1.28$, the instability phenomenon occurs on the surface of the cavity. By extracting the contour of the cavity at the moment of breaking, and considering that the cavity is an axisymmetric shape, the volume change in the cavity was further calculated, as shown in Figure 11.

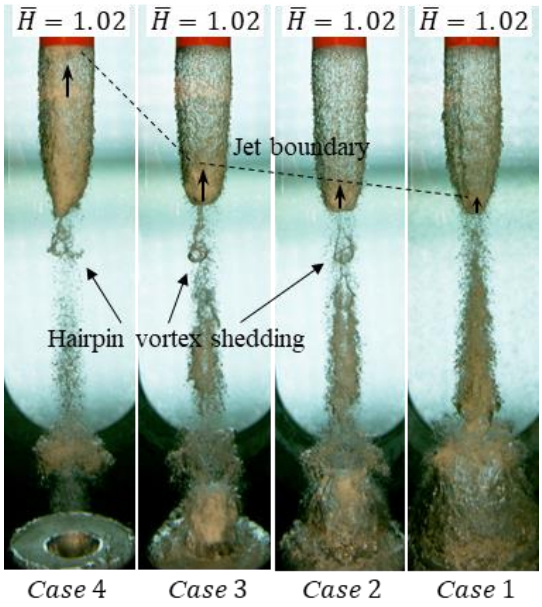


Figure 10. Under the same water depth and different ventilation flow rates, the impact shape of cavity jet.

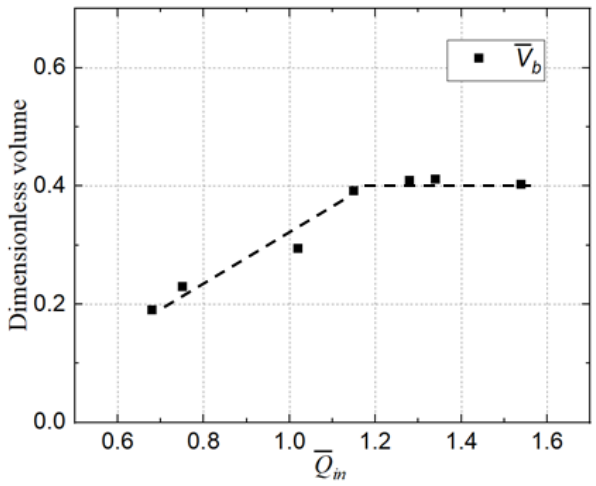


Figure 11. Volume of attached cavity varies with ventilation.

As shown in Figure 11, the overall shape of the tail attachment cavity is not much different, and the volume difference is very small. This shows that in the early stage of cavity breaking, the adhesion of gas to the bottom of the vehicle has not changed. Under the condition of a certain cavitation number, the total amount of gas that can be adsorbed at the tail of the vehicle is constant. The volume of the attached cavity at the tail of the vehicle cannot be increased.

According to the change curve of cavity length under different ventilation flow rates, as shown in Figure 12, it can be found that the cavity length experienced a decreasing trend in the initial stage, and then the cavity length increased with a sudden drop. This is because the length of the tail attachment cavity is the largest at the moment of breaking, and the size of the cavity is reduced due to the shrinkage of the cavity after the breaking because the internal pressure of the cavity is lower than the external pressure. At the same time, the length mutation caused by the shedding of terminal bubbles occurred during the movement. It can be found that with the increase in ventilation flow, the frequency of cavity shedding also decreases. On the other hand, the air mass at the mouth of the barrel increases with the increase of the ventilation flow rate, and most of the gas stays at the mouth of the launching barrel. However, the length of the cavity at the tail of the vehicle does not change significantly with the ventilation flow rate, which indicated that the factor of ventilation flow rate had little influence on the cavity length. The Strouhal numbers are $St = 0.402$, $St = 0.355$, $St = 0.905$, and $St = 1.283$. It can be observed that the degree of dispersion of Strouhal number is important, which is mainly due to the uncertainty in the length caused by bubble shedding.

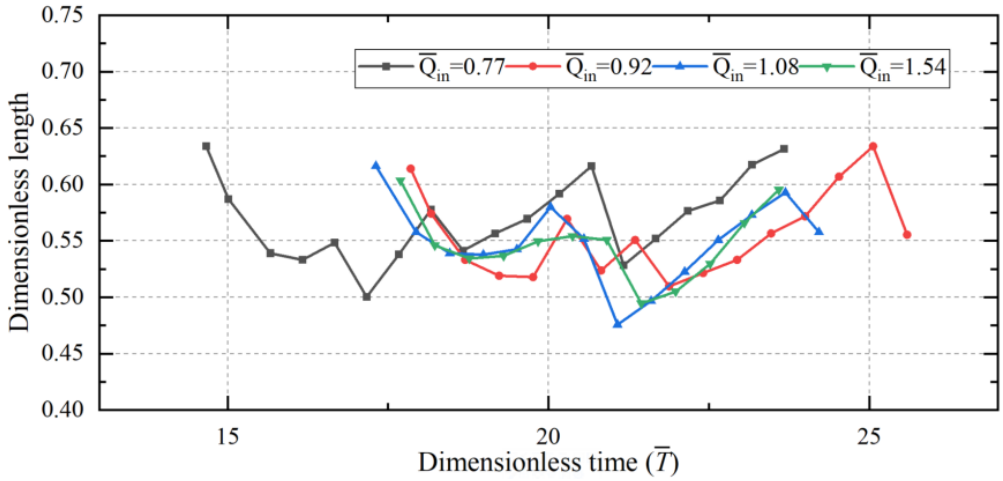


Figure 12. Variation curve of cavity length with the displacement of vehicle under different ventilation flow rates.

In fact, every decrease in the length of the cavity indicates that the cavity is shedding. Further spectrum analysis of the cavity shedding period was conducted, as shown in Figures 13 and 14. It can be found that under different ventilation flow rates, the maximum amplitude of cavity shedding is near 50 Hz in the low frequency region. By summarizing the cavity shedding frequency under different ventilation flow rates, it can be found that the shedding frequency presents a trend of first increasing and then decreasing.

3.3. Effect of Cavitation Number on the Flow Pattern of Tail Attachment Cavity

Cavitation number, the main influencing factor in cavity flow, has an important influence on the characteristics of cavity flow. In this study, the effect of the cavitation number on the shape of the cavity was evaluated by changing the gas pressure above the liquid surface. Therefore, cases 5–7 were selected to better evaluate the influence of the cavitation number on the cavity morphology. Figures 15 and 16 show the cavity breaking shape of vehicle under different cavitation numbers and the formation mechanism of the jet after breaking. From the figure, we can observe that with the increase in the cavitation number, the breaking position of the cavity also decreases, and the jet impact becomes more obvious. This is due to a decrease in the cavitation number, resulting in a smaller pressure gradient in the flow field and an increase in the cavity length.

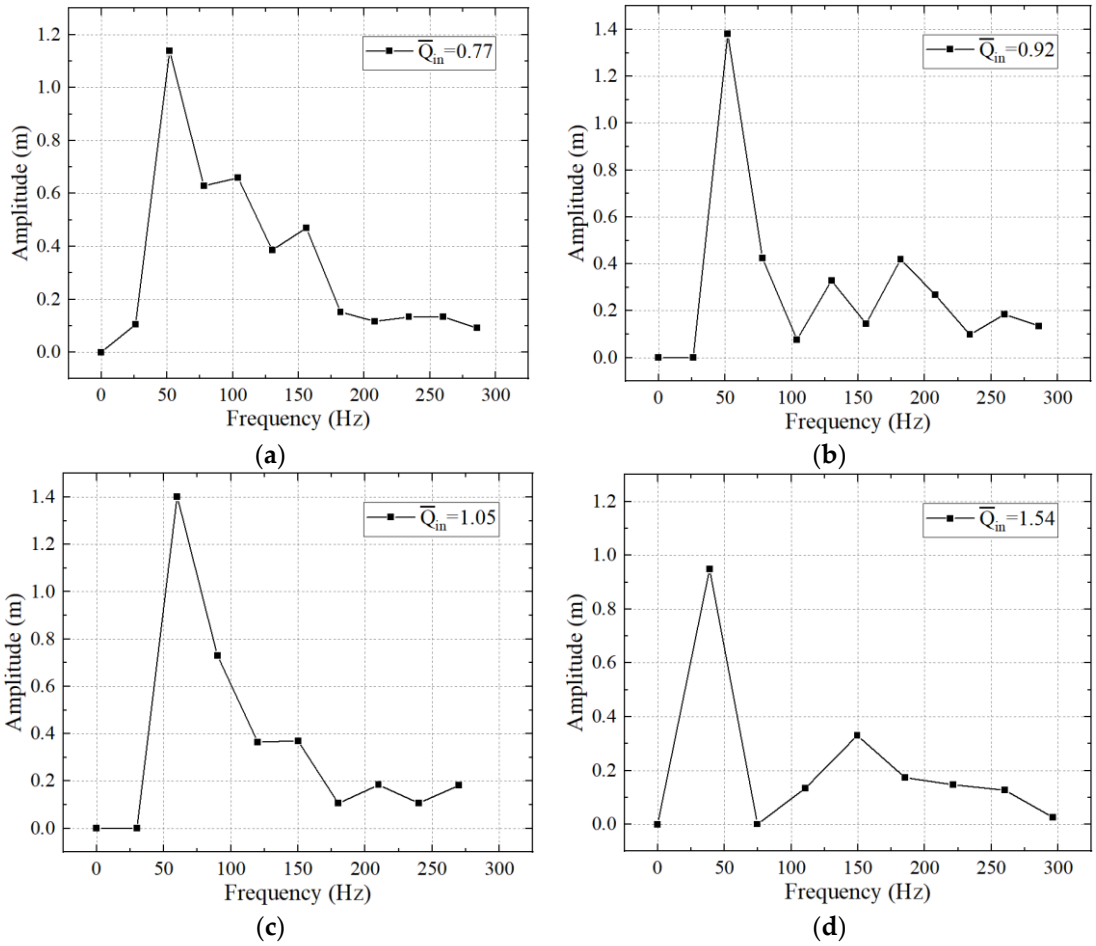


Figure 13. Spectrum analysis of cavity length at different ventilation flow rates. Where (**a**–**d**) are the spectrum analysis of cavity length at $\overline{Q}_{in}$ = 0.77, 0.92, 1.05 and 1.54, respectively.

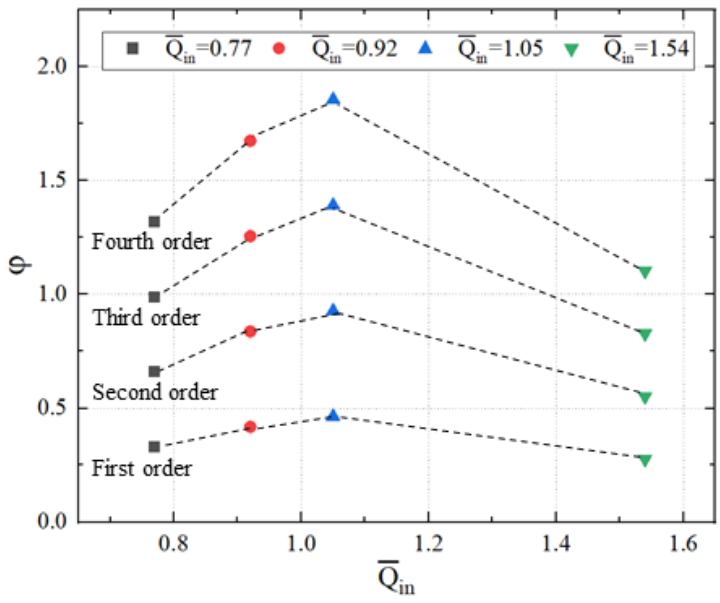


Figure 14. Relationship between different ventilation flow rates and cavity shedding frequency.

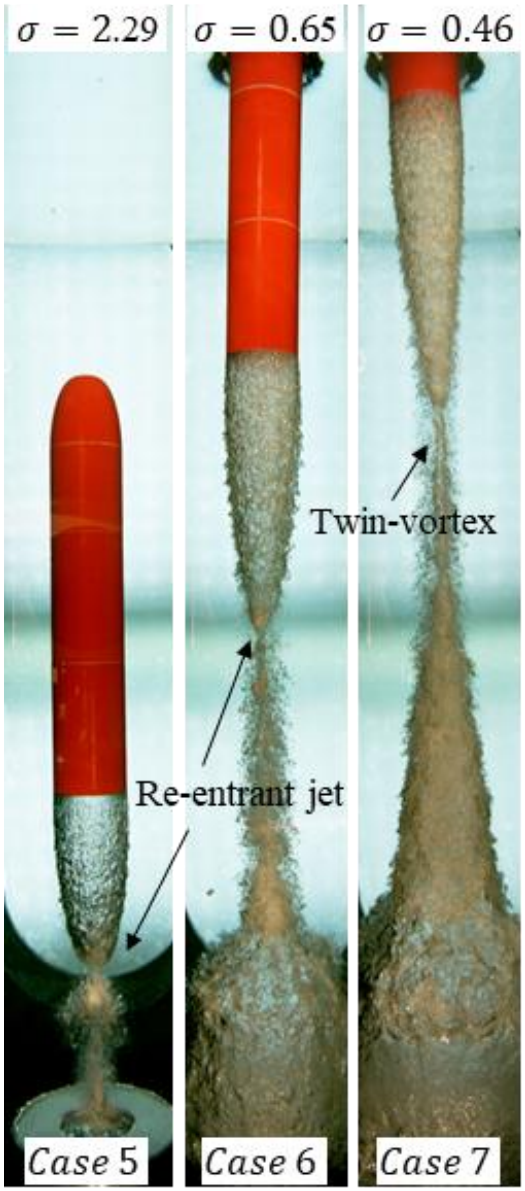


Figure 15. Cavitation morphologies of three working conditions under different cavitation numbers. The breaking positions are located at $\overline{H}$ = 1.86, 0.78, and 0.15.

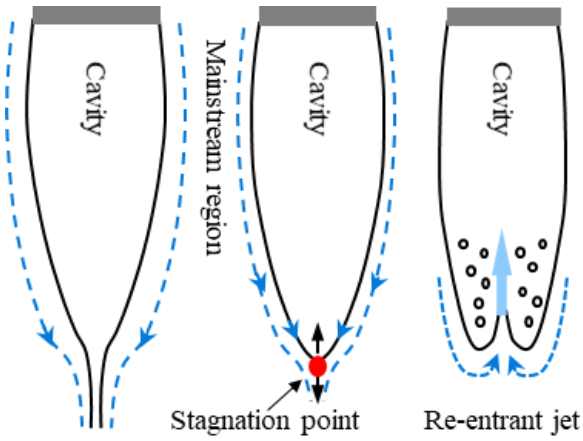


Figure 16. Formation mechanism of re-entrant jet.

It can be observed from the mechanism diagram that the fracture of the cavity is pinched off by the streamline at the smallest diameter, and the fracture of the cavity is closed to form a stagnation point. Because the internal pressure is lower than the ambient pressure when the bubble is broken, the balance of inertial force and pressure causes the bubble to bend inward, promoting the liquid to be injected into the bubble and form a re-entrant jet. A smaller pressure gradient makes the cavity lead to breaking. The circumferential water body squeeze force on the columnar cavity is small, and the formed stagnation point pressure is small, thus generating a small pressure difference with the internal pressure of the cavity. Therefore, the formed re-entrant jet impingement phenomenon is weak.

Through further statistics on the change of cavity length under different cavitation numbers, as shown in Figure 17, it was found that with the decrease in the cavitation number, the length of breaking time of the cavity also increases. The smaller the cavitation number, the smaller the water depth, and the smaller the variation in the cavity length. However, under a large cavitation number, due to the effect of bubble shedding, the change amplitude of the cavity length is larger.

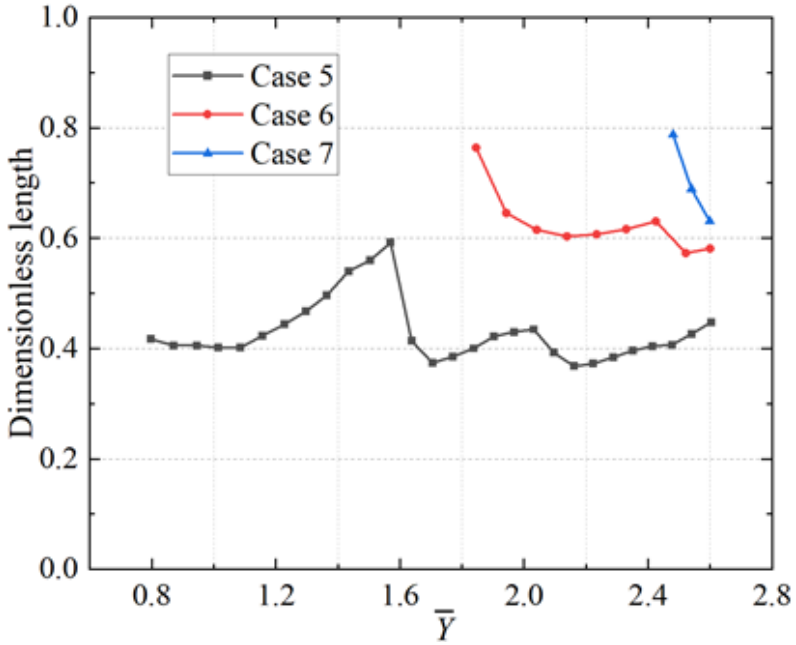


Figure 17. Variation curve of cavity length with displacement under different cavitation numbers.

In addition, we also observed two special cavity flow patterns at low cavitation numbers in cases 8 and 9, as shown in Figures 18 and 19. When the ventilation volume and Froude number are both at low levels, the air mass at the outlet of the launcher is completely entrained into the cavity, forming a giant spindle cavity (GSC) with bubbles on the surface. The cavitation number and Froude number are $\sigma = 0.86$ and $Fr = 8.34$, respectively. In case 9, when the ventilation volume increases and the Froude number increases, the columnar cavity is torn from the center and gradually expands to form two tubular air columns at the tail of FTC. With the vertical motion of the vehicle, a twin-vortex deflated mode (FTC-TV) under an FTC is formed. The cavitation number and Froude number are $\sigma = 0.21$ and $Fr = 16.9$, respectively.

It can be observed that in the formation of GSC, almost all the air mass at the outlet of the launcher is entrained into the cavity, and there is almost no gas left at the outlet of the launcher, thus forming a cavity shape whose size is much larger than that of the underwater vehicle. At the same time, there is a convex and uneven cavity distribution on the cavity surface, which is mainly due to the large radial size of the cavity and the bulge on the cavity surface under the shear action of incoming flow. Compared with the twin-vortex venting mode under the FTC, the radial size of the cavity is much smaller, because the scouring

effect of the incoming flow is intensified under a high Froude number. Thus, the radial size of the cavity cannot be maintained. Figure 20 shows the flow pattern distribution of the tail attachment cavity with ventilation under different cavitation numbers.

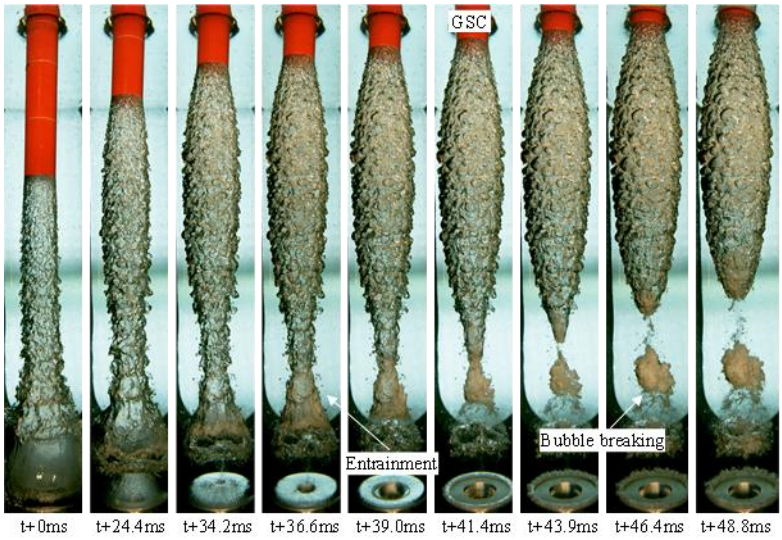


Figure 18. Formation and development of GSC in case 8.

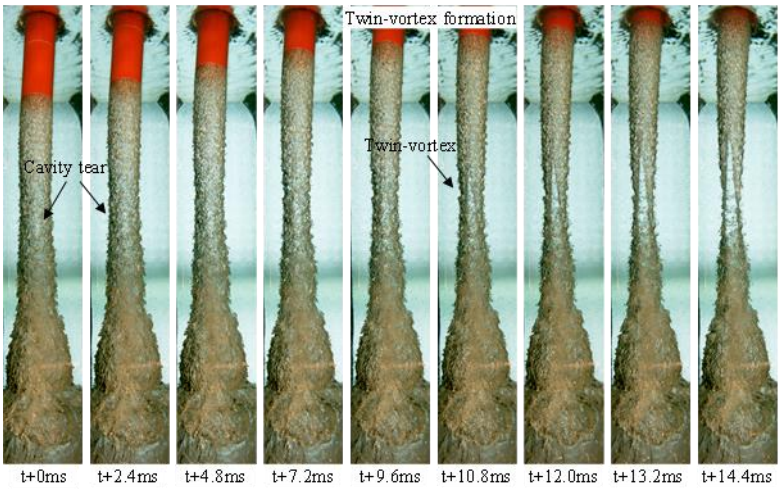


Figure 19. Formation and development of FTC-TV in case 9.

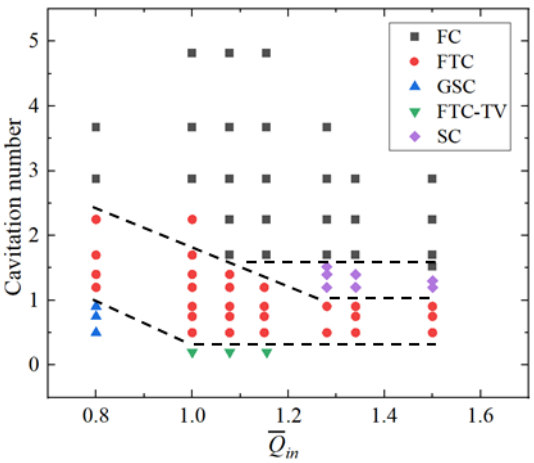


Figure 20. Map of different flow patterns for tail attachment cavity.

Figure 20 shows that under different ventilation volumes, the cavity morphology has experienced the evolution of FTC-FC. Among them, the GSC only appeared at a low cavitation number and small ventilation volume. With the increase in ventilation volume, the FTC-TV cavity mode appeared. The shrinkage cavity (SC) exists in the transitional stage of transition between the transparent cavity FTC and FC, and only exists in the working condition of a large ventilation volume. When the attached cavity is close to the water surface, the FC appears, because the velocity decreases near the free liquid surface. At the same time, under the impact of the jet, the air and water are strongly mixed, which makes the cavity appear foamy.

To study the tail attachment cavities, the length of the cavity has always been the key research object because its vertical unsteady motion characteristics are different from the horizontal cavity shape in the water tunnel test. Through the statistics of the length of the cavity at the closing moment, as shown in Figure 21, it can be found that the length of the cavity increases with the decrease in the cavitation number at the closed position, and the two have a linear relationship on the whole.

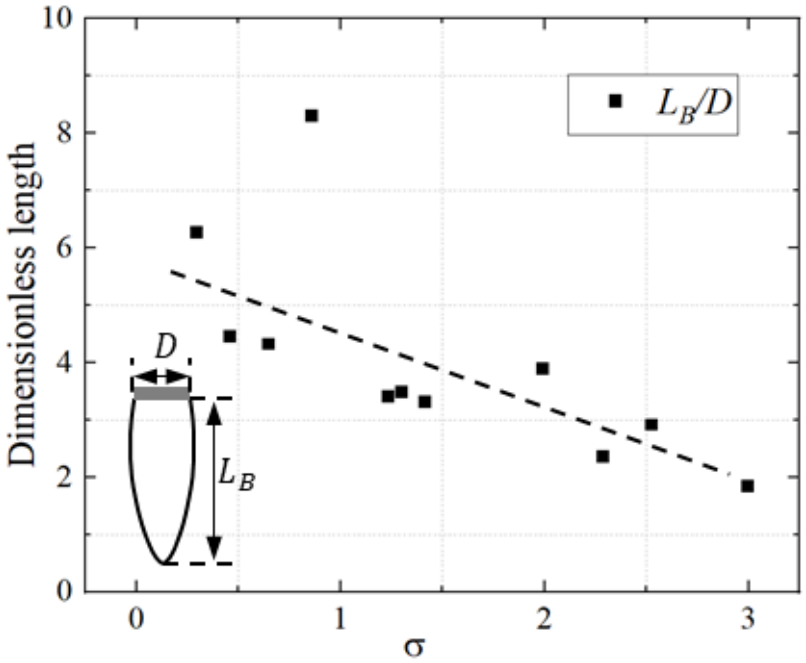


Figure 21. Length of cavity length with cavitation number when the cavity is closed.

4. Conclusions

Through the self-designed aerodynamic ejection device, this study realized the free underwater movement of the vehicle, captured the formation mechanism and pressure fluctuation characteristics of the tail attachment cavity during the vehicle movement, and summarized the flow characteristics under different ventilation rates and cavitation numbers. Through the comparative analysis of experiments, the following conclusions can be drawn:

(1) Under the circumstance of a Froude number and the diameter of the vehicle, the capacity of the independent cavity volume attached to the tail of the vehicle remains constant, and a continuous increase in the ventilation volume cannot increase the volume of the tail attachment cavity.

(2) When the cavitation number is increased, the position where the tail attachment cavity breaks is also reduced, and the jet impact phenomenon is more obvious. At the same time, the length of the cavity increases with the decrease in the cavitation number, and the two generally have a linear relationship.

(3) When the ventilation volume reaches a critical value $\overline{Q}_{in} = 1.28$, the cavity pulsation phenomenon occurs, and is accompanied by a strong jet impact. The maximum impact pressure peak is about 1.2–1.4 times of the local pressure, and the pulse width is about 0.4 ms.
(4) Reducing the cavitation number can reduce the pressure gradient and reduce the pressure difference between inside and outside the cavity, thereby reducing the occurrence of jet impingement.

Author Contributions: Conceptualization and methodology, all authors; writing—original draft preparation, Z.Q.; writing—review and editing, X.Y. and G.M.; project administration, N.Y.; funding acquisition, X.Q. and S.C. All authors have read and agreed to the published version of the manuscript.

Funding: This work is supported by National Natural Science Foundation Enterprise Innovation and Development Joint Fund (Grant No. U20B2005), National Natural Science Foundation of China (Grant No. 52271308), National Natural Science Foundation of China (Grant No. 52001095), and National Defense Basic Scientific Research program of China (Grant No. JCKY2021604B028).

Institutional Review Board Statement: Not applicable.

Informed Consent Statement: Not applicable.

Data Availability Statement: The original data contributions presented in the study are included in the article; further inquiries can be directed to the corresponding authors.

Conflicts of Interest: The authors declare no conflict of interest.

References

1. Karn, A.; Arndt, R.; Hong, J. An experimental investigation into supercavity closure mechanisms. *J. Fluid Mech.* **2016**, *789*, 259–284. [CrossRef]
2. Zhou, L.; Yu, Y. Study on interaction characteristics between multi gas jets and water during the underwater launching process. *Exp. Therm. Fluid Sci.* **2017**, *83*, 200–206. [CrossRef]
3. Weiland, C.; Vlachos, P.P. Round gas jets submerged in water. *Int. J. Multiph. Flow* **2013**, *48*, 46–57. [CrossRef]
4. Yang, J.; Teng, P.; Zhang, H. Experiments and CFD modeling of high-velocity two-phase flows in a large chute aerator facility. *Eng. Appl. Comput. Fluid Mech.* **2019**, *13*, 48–66. [CrossRef]
5. Shi, Y.; Ren, J.; Gao, S.; Pan, G. Numerical Investigation on Air Film Fusion of Pressure-Equalizing Exhaust around Shoulder Ventilation of Submarine-Launched Vehicle. *J. Mar. Sci. Eng.* **2022**, *10*, 39. [CrossRef]
6. Quan, X.; Cheng, S. Experimental and numerical investigation on the gas leakage regime for ventilated tail cavity of an underwater vehicle. *J. Hydrodyn.* **2023**, *35*, 46–60. [CrossRef]
7. Shi, H.; Wang, B.; Dai, Z. Research on the mechanics of underwater supersonic gas jets. *Sci. China Phys. Mech. Astron.* **2010**, *53*, 527–535. [CrossRef]
8. Dong, P.; Lu, B.; Gong, S.; Cheng, D. Experimental study of submerged gas jets in liquid cross flow. *Exp. Therm. Fluid Sci.* **2020**, *112*, 109998. [CrossRef]
9. Mao, N.; Kang, C.; Ding, K.; Cao, Q. Gas-liquid two-phase flow patterns in the wake of a submerged nozzle under co-flow condition. *Int. J. Multiph. Flow* **2021**, *138*, 103604. [CrossRef]
10. Huang, R.; Qiu, R.; Zhi, Y.; Wang, Y. Investigations into the ventilated cavities around a surface-piercing hydrofoil at high Froude numbers. *Phys. Fluids* **2022**, *34*, 043304. [CrossRef]
11. Bhaga, D.; Weber, M.E. Bubbles in viscous liquids: Shape, wakes and velocities. *J. Fluid Mech.* **1981**, *105*, 61–85. [CrossRef]
12. Clift, R.; Grace, J.R.; Weber, M.E. *Bubbles, Drops and Particles*; Academic Press: Cambridge, MA, USA, 1978.
13. Coutanceau, M.; Thizon, P. Wall effect on the bubble behaviour in highly viscous liquids. *J. Fluid Mech.* **1981**, *107*, 339–373. [CrossRef]
14. Shao, S.; Wu, Y.; Haynes, J.; Arndt, R.E.A.; Hong, J. Investigation into the behaviors of ventilated supercavities in unsteady flow. *Phys. Fluids* **2018**, *30*, 052102. [CrossRef]
15. Xiao, Z.; Tan, R. Theoretical modeling of bubbling regimes in bubble formation with bubble–bubble and bubble–wall interactions. *J. Chem. Eng. Jpn.* **2008**, *41*, 453–459. [CrossRef]
16. Wei, Y.J.; Cao, W.; Wang, C.; Zhang, J.Z.; Zou, Z.Z. *New Trends in Fluid Mechanics Research*; Zhuang, F.G., Li, J.C., Eds.; Springer: Berlin/Heidelberg, Germany, 2007.
17. Ceccio, S.L. Friction drag reduction of external flows with bubble and gas injection. *Annu. Rev. Fluid Mech.* **2010**, *42*, 183–203. [CrossRef]
18. Jiang, Y.; Jeong, S.-W.; Ahn, B.-K.; Kim, H.-T.; Jung, Y.-R. Experimental investigation of drag characteristics of ventilated supercavitating vehicles with different body shapes. *Phys. Fluids* **2019**, *31*, 052106. [CrossRef]

19. Wang, G.; Kong, D.; Wu, Q.; Liu, T.; Zheng, Y.; Huang, B. Physical and numerical study on unsteady shedding behaviors of ventilated partial cavitating flow around an axisymmetric body. *Ocean Eng.* **2020**, *197*, 106884. [CrossRef]
20. Liu, T.; Huang, B.; Wang, G.; Zhang, M.; Gao, D. Experimental investigation of the flow pattern for ventilated partial cavitating flows with effect of Froude number and gas entrainment. *Ocean Eng.* **2017**, *129*, 343–351. [CrossRef]
21. Shereena, S.G.; Vengadesan, S.; Idichandy, V.G.; Bhattacharyya, S.K. CFD study of drag reduction in axisymmetric underwater vehicles using air jets. *Eng. Appl. Comput. Fluid Mech.* **2013**, *7*, 193–209. [CrossRef]
22. Sun, T.; Zhang, X.; Xu, C.; Zhang, G.; Wang, C.; Zong, Z. Experimental investigation on the cavity evolution and dynamics with special emphasis on the development stage of ventilated partial cavitating flow. *Ocean Eng.* **2019**, *187*, 106140. [CrossRef]
23. Sun, T.; Ding, Y.; Huang, H.; Xie, B.; Zhang, G. Numerical study on the effects of modulated ventilation on unsteady cavity dynamics and noise patterns. *Phys. Fluids* **2021**, *33*, 123307. [CrossRef]
24. Xu, H.; Wang, C.; Lu, H.-Z.; Huang, W.-H. Experimental study on submerged supersonic gaseous jet induced tail cavity. *Acta Phys. Sin.* **2018**, *67*, 014703. [CrossRef]
25. Candon, S.; Marshall, J.S. Vortex ring deformation, capture, and entrainment by a columnar vortex. *Phys. Fluids* **2012**, *24*, 093604. [CrossRef]
26. Yoon, K.; Qin, S.; Shao, S.; Hong, J. Internal flows of ventilated partial cavitation. *Exp. Fluids* **2020**, *61*, 100. [CrossRef]
27. Hao, L.; Kong, D.; Wu, Y.; Liu, T.; Wang, G. Transition and gas leakage mechanisms of ventilated cavities around a conical axisymmetric body. *Phys. Rev. Fluids* **2022**, *7*, 123901. [CrossRef]
28. Qu, Z.; Yang, N.; Ma, G.; Yao, X.; Chen, Y. Experimental study of unsteady evolution characteristics of ventilated air mass on the cylinder surface. *Ocean Eng.* **2022**, *264*, 112462. [CrossRef]
29. Moudjed, B.; Excoffon, J.; Riva, R.; Rossi, L. Experimental study of gas entrainment from surface swirl. *Nucl. Eng. Des.* **2016**, *310*, 351–362. [CrossRef]
30. Spurk, J.H. Effect of gas temperature on the gas loss from ventilated cavities. *Acta Mech.* **2004**, *172*, 75–81. [CrossRef]
31. Yu, A.; Qian, Z.; Wang, X.; Tang, Q.; Zhou, D. Large Eddy simulation of ventilated cavity with an insight on the correlation mechanism between ventilation and vortex evolutions. *Appl. Math. Model.* **2021**, *89*, 1055–1073. [CrossRef]
32. Kinzel, M.P.; Krane, M.H.; Kirschner, I.N.; Moeny, M.J. A numerical assessment of the interaction of a supercavitating flow with a gas jet. *Ocean Eng.* **2017**, *136*, 304–313. [CrossRef]
33. Jiang, Y.; Shao, S.; Hong, J. Experimental investigation of ventilated supercavity with gas jet cavitator. *Phys. Fluids* **2018**, *30*, 012103. [CrossRef]
34. Gan, N.; Liu, Y.; Yao, X.; Chen, Y.; Ma, G.; Cui, X. Experimental investigation on the development features of a gas jet on the surface of a vertical moving body with a constant volume chamber. *Phys. Fluids* **2022**, *34*, 083313. [CrossRef]

Disclaimer/Publisher's Note: The statements, opinions and data contained in all publications are solely those of the individual author(s) and contributor(s) and not of MDPI and/or the editor(s). MDPI and/or the editor(s) disclaim responsibility for any injury to people or property resulting from any ideas, methods, instructions or products referred to in the content.